REMBRANDT BASIN: DISTINGUISHING BETWEEN VOLCANIC AND IMPACT-PRODUCED SMOOTH PLAINS DEPOSITS ON MERCURY. Jennifer L. Whitten[1], James W. Head[1], Jörn Helbert[2], and Sean C. Solomon[3,4], [1]Department of Geological Sciences, Brown University, Providence, RI 02912, USA, *jennifer_whitten@brown.edu*; [2]Institute for Planetary Research, Deutsches Zentrum für Luft- und Raumfahrt, Rutherfordstrasse 2, Berlin, Germany; [3]Lamont-Doherty Earth Observatory, Columbia University, Palisades, NY 10964, USA; [4]Department of Terrestrial Magnetism, Carnegie Institution of Washington, Washington, DC 20015, USA.

Introduction: Rembrandt basin (~715 km diameter; center at 33°S, 88°E) is the second-largest well-preserved basin on Mercury [1, 2]. Massifs in the northern interior of the basin hint at an interior ring ~450 km in diameter. The basin deposits bear a striking similarity to the Hevelius and Montes Rook formations in the lunar Orientale basin; interior smooth plains deposits also bear similarities to Lacus Autumni, Lacus Veris, and Mare Orientale [e.g., 3]. In addition to the preservation of the basin deposits, the crater size-frequency distribution for Rembrandt indicates a relatively young basin age, comparable to that of the larger Caloris basin [1, 2].

Surface reflectance data from the Mercury Atmospheric and Surface Composition Spectrometer (MASCS) instrument on the MErcury Surface, Space ENvironment, GEochemistry, and Ranging (MESSENGER) spacecraft indicate that the characteristics of Rembrandt interior deposits differ from those of surrounding terrain [4-6]. By several metrics the Rembrandt interior smooth plains appear similar to the northern smooth plains [4-6]. However, the exterior deposits show more similarities to low-reflectance material (LRM) [7]. LRM is thought to represent a subsurface deposit that is emplaced onto the surface as crater and basin ejecta [7].

The abundance of well-preserved smooth plains deposits within Rembrandt and their anomalous spectral signatures prompted us to investigate their distribution and origin. We addressed the following questions in our study: (1) Are there different smooth plains morphologies within and around Rembrandt basin? (2) What are their distributions? (3) What can color and spectral variations and stratigraphic relationships tell us about their dominant formation process (volcanism [e.g., 8, 9] versus generation as fluidized impact deposits [e.g., 10, 11]) and the sequence of activity within and around the Rembrandt basin?

Methods: Mercury Dual Imaging System (MDIS) data were used for the mapping portion of this project. Initially, a map of the smooth plains was produced from a MDIS 250 m/pixel albedo map. This map was helpful in distinguishing between plains deposits of high and low albedo. The smooth plains were mapped on the basis of an earlier unit definition [9]. An MDIS 250 m/pixel high-incidence-angle map was also used to aid in the morphologic identification of smooth plains. This product was especially helpful in identifying smooth plains exterior to Rembrandt basin. Only the largest deposits (those >20 km in horizontal extent) were mapped for this study.

Results: We identified three different smooth plains units within and around Rembrandt basin (Fig. 1): (1) a high-albedo plains unit similar to high-reflectance red plains (HRP) [7], (2) a low-albedo unit, and (3) a hummocky low-albedo unit. The hummocky unit is confined to the northern interior of the basin (Fig. 1a); on the Moon a similar morphologic unit, known as the Montes Rook Formation, is observed in the well-preserved Orientale basin between the outer scarp ring (the Cordillera Mountains) and the rim crest of the basin transient cavity (the Outer Rook Mountains) and has been interpreted as a product of transient cavity collapse [12, 13]. The high-albedo units occur both within and exterior to the basin (Fig. 1a); those high-albedo plains exterior to the basin are found within craters and as large continuous deposits in low-lying terrain. The majority of the low-albedo smooth plains are located exterior to Rembrandt; these plains tend to contain more wrinkle ridges than the high-albedo deposits, especially to the east of the basin.

Discussion: A comparison of our map with the global color units [7] shows good correlation for the high-albedo units. However, our low-albedo unit overlaps with both the LRM and low-reflectance blue plains (LBP) MDIS color units, indicating that our low-albedo plains may need to be further subdivided. The substantial overlap between our low-albedo unit and the LBP unit suggests that these deposits exterior to Rembrandt may have formed by processes similar to those responsible for the large deposits of LBP around Caloris basin.

The mapped plains deposits from this study also correlate well with variations in spectral reflectance seen in Mercury Atmospheric and Surface Composition Spectrometer (MASCS) data [14] (Fig. 2), increasing confidence in our map units and also supporting a possible compositional difference between the high- and low-albedo deposits. Including the Visible and Infrared Spectrograph (VIRS) component (320–1450 nm) of the MACSCS data reveals an additional spectral unit in the high-albedo smooth plains in the basin interior (Fig. 2, orange). The VIRS data indicate that the textured rim material of Rembrandt basin (Fig. 2, dark blue) has

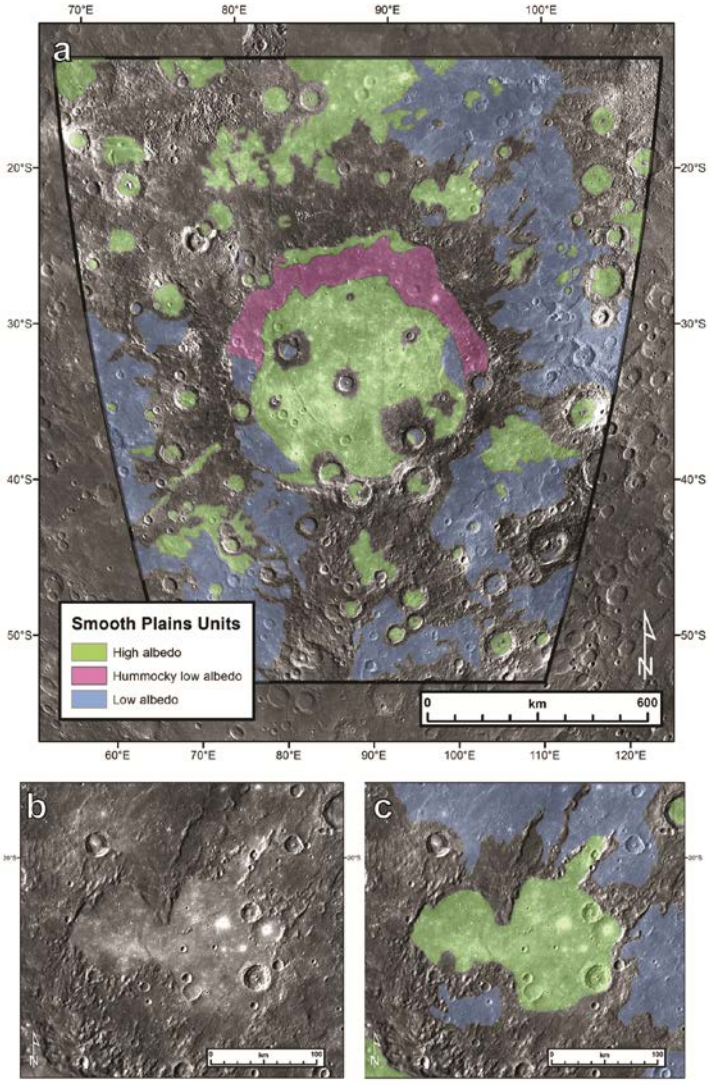

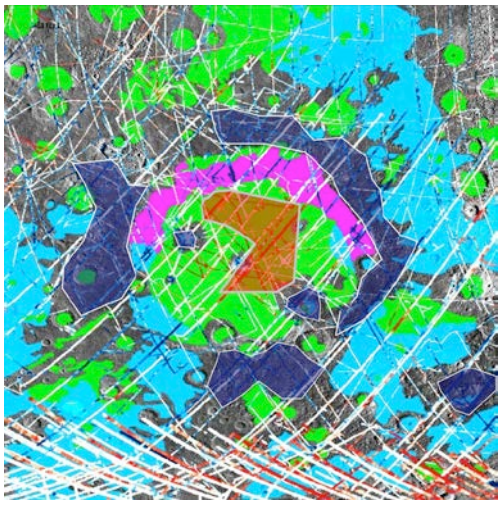

Figure 1 (left). Map of the smooth plains units within and around Rembrandt basin identified in this study. (a) Regional view showing the distribution of all three plains units. (b) Close-up view of high-albedo plains to the northeast of the basin rim. (c) Same as (b), but with the geologic map overlaid.

Figure 2 (top). Classification of spectral reflectance from MASCS VIRS data at high ratios of signal to noise [15]. The green and light-blue units correspond to the high-albedo and low-albedo units of Fig. 1. The pink unit corresponds to the hummocky low-albedo unit of Fig. 1. Two additional spectral units (orange and dark blue) are distinctive on the basis of spectral slope in the UV. Lines are tracks of MASCS data color coded for reflectance at 350 nm wavelength (white = spectrally neutral deposits, red = comparatively red-sloped spectra, blue = comparatively blue-sloped spectra. (Courtesy of J. Helbert).

spectral properties similar to the low-albedo smooth plains. This similarity supports the interpretation that the latter unit is dominated by basin ejecta material.

The stratigraphic relationships between the high-albedo smooth plains and the low-albedo smooth plains help to address the formation mechanism and the relative timing of these events. For instance, to the northeast of Rembrandt basin there is a high-albedo deposit located within two overlapping impact craters (Fig. 1b, c). The rims of these two craters are modified by basin ejecta deposits (as indicated by the linear striations radial to the basin center) and have an albedo similar to textured basin ejecta. Subsequently, these craters were filled with high-albedo smooth plains that are interpreted to be volcanic on the basis of their distinctive color, their embayment of low-lying topography, and superposition on recognized basin-related deposits [e.g., 7]. Numerous other areas surrounding Rembrandt basin provide excellent examples of these same relationships between the high-albedo (interpreted to be volcanic) and low-albedo (generally interpreted to be basin-related) smooth plains. Thus, the combination of albedo variations and embayment relationships can help to distinguish between volcanically emplaced smooth plains and impact-produced smooth plains (impact melt or ponded ejecta) where these types of clear relations exist.

References: [1] Watters T. R. et al. (2009) *Science, 324*, 618–621. [2] Fassett C. I. et al. (2012) *JGR, 117*, E00L08. [3] Whitten J. L. et al. (2010) *JGR, 116*, E00G09. [4] Helbert J. et al. (2013) *LPS, 44*, abstract 1496. [5] Izenberg N. R. (2014) *Icarus, 228*, 364–374. [6] D'Amore M. et al. (2014) *LPS, 45*, submitted. [7] Denevi B. W. et al. (2009) *Science*, 324, 613–618. [8] Strom R. G. (1977) *JGR, 80*, 2478–2507. [9] Denevi B. W. et al. (2013) *JGR, 118*, 891–907. [10] Wilhelms D. E. (1976) *Icarus, 28*, 551–558. [11] Oberbeck V. R. et al. (1977) *JGR, 82*, 1681–1698. [12] Head J. W. (1974) *Moon, 11*, 327–356. [13] Head J. W. (2010) *GRL, 37*, L02203. [14] Helbert J. et al. (2013) *GSA Abstracts with Program, 45*, 383. [15] D'Amore M. et al. (2013) *LPS, 44*, abstract 1900.